Mathematical-physical analysis of the generic dual-dipole antenna

Version 7

J.P. Hamaker

August 31, 2011

File:.../pol/antennas/analDD.rno

History

1. 2007: Original version: Basic beam model; reduced-beam concept; single-frequency Jones and Mueller matrix expansions in θ, ϕ; antenna rotation and tilting (later shelved).
2. August 2008: General upgrade. Sections anticipating later needs shelved. **P**-matrix expansion in double (θ, f) polynomial (Sec. 7). Model fitting with equal relative error over the beam (App. B.2).
3. September 10, 2008: Interferometer response to unpolarized source (later shelved).
4. March 2009: Miscellaneous textual corrections and clarifications. Reduced beam for LOFAR station (later discarded).
5. July 2009: Overall gain modeling (Sec. 5).
6. August 2009: Mueller-matrix beam, raw and including effect of parallactic rotation; rediction of Stokes output vs HA (Sec. 8). Prediction of Stokes outputs vs hour angle. Calculation of Mueller matrix (App. D).
7. September 1 2009: Definitions of dipole orientations (Secs. 5.3 and 8.5).

Contents

Appendix

Abstract

This document collects various approaches to the description of a dual-dipole antenna that have earlier been laid down in preliminary notes. It is meant to supersede these notes and to tie up a number of ends that were left loose earlier.

From a basic physical symmetry consideration an analytic series expression is derived for the Jones-matrix beam pattern $\mathbf{J}(\theta, \phi)$. The coefficients in this expression can be found by fitting to a numerically simulated beam raster of the type generated for LOFAR by Astron's Antenna Group.

The expression is then applied in several ways to study the properties of the dual-dipole antenna pattern (cf. the table of contents):

- Representing the beam for arbitrary sky directions and plotting it.
- Studying various aspects of the Mueller-matrix beam for an interferometer.
- Studying options to vary azimuthal antenna orientations within a station
- Studying the effect of heterogeneity in the LOFAR array: antenna tilts and rotations of antenna azimuths per station.

Where possible, a fully analytic approach is taken. Where this leads to an unwieldy development, qualitive reasoning is supplemented by numeric calculations.

The antenna beam described here is a smooth sky-wide envelope that must be multiplied with a station array beam that has a much finer directional structure. In the product, the antenna beam represents a gradient over the main beam that is less than some 10% of the beam peak. This gradient may be readily absorbable in a station beam model designed to model just the array beam.

Thus the value of the antenna-beam model to be presented here is not so much in its details as it is in its qualitative description, particularly of its azimuth dependence.

1 Introduction

The aim of this Note is to represent the antenna pattern of a generic LOFAR dual-dipole by an analytic model. The geometry of the antennas is too complex to be tractable on the basis of Maxwell's equations. Consequently, the only data we have are numerical simulations, based on those equations, that have been made by the Antenna Group (M.J. Arts).

On the theoretical side, the geometrical symmetries in the assembly of two mutually perpendicular dipoles dictate corresponding azimuthal symmetries in the analytic antenna model. In the frequency domain, the antennas have been designed to be resonant somewhere near the band centre; in addition their effective surface should be proportional to $1/\lambda^2 \propto f^2$ for wavelengths exceeding their size.

All of these features are found to be present in the simulated antenna patterns, thus providing a justification for the theory-based approach to be taken in this Note.

2 Limitations and reservations

The simulated data represent a single antenna with ground plane on a flat Earth remote from electromagnetic obstructions, neighbouring antennas in particular. Such obstructions subvert the symmetries of the lone antenna, introducing even ϕ harmonics and modifying the pattern in other ways.

Such obstructions are omnipresent in the form of neighbouring antennas. Little is known about the affects of mutual coupling between them: Proper e.m. simulation of a realistically populated antenna array is computationally not feasible. Analytical approximations strictly work only for regular antenna arrays of infinite size, but may yield a good approximation for the HBA stations. For the LBA the effect of coupling remains a great question mark. It is hoped that an average antenna pattern will emerge that is similar to the pattern of the lone antenna so the latter can be used as a starting point for describing the main station beam. For the sidelobes

this will most probably not be the case, but the received wisdom is that there will be no need to describe them accurately.

All in all, the relevance of this Note remains to be seen. At present it represents work in progress. Some of the studies conducted to date will only be included later when they are expected to become relevant. The History on the title page represents the development.

3 Basic concepts

4 Some necessary terminology

The combination of two mutually perpendicular, nominally horizontal dipoles, is the basic antenna element of LOFAR. Following what now seems to be standard LOFAR terminology, we shall refer to this unit simply as an *antenna*. Starting from elementary physics, this Note develops a model in which it is descibed as an atomic unit.

The response of the antenna to a source is a continuous Jones-matrix function $\mathbf{J}$ of source position (θ, ϕ). This function will be referred to as the antenna's *beam*.

We shall demonstrate that it is possible in software to create a virtual antenna that approximately tracks a point source in azimuth, i.e. it simulates the effect of rotating the true antenna. The pattern of this virtual antenna will be called the *reduced* beam.

In observing an extended field, an obvious first processing step is to divide an observed coherency by the beam's Jones matrix for the field centre. This *normalisation* is equivalent to gain normalisation for a scalar instrument.

5 The modeling procedure

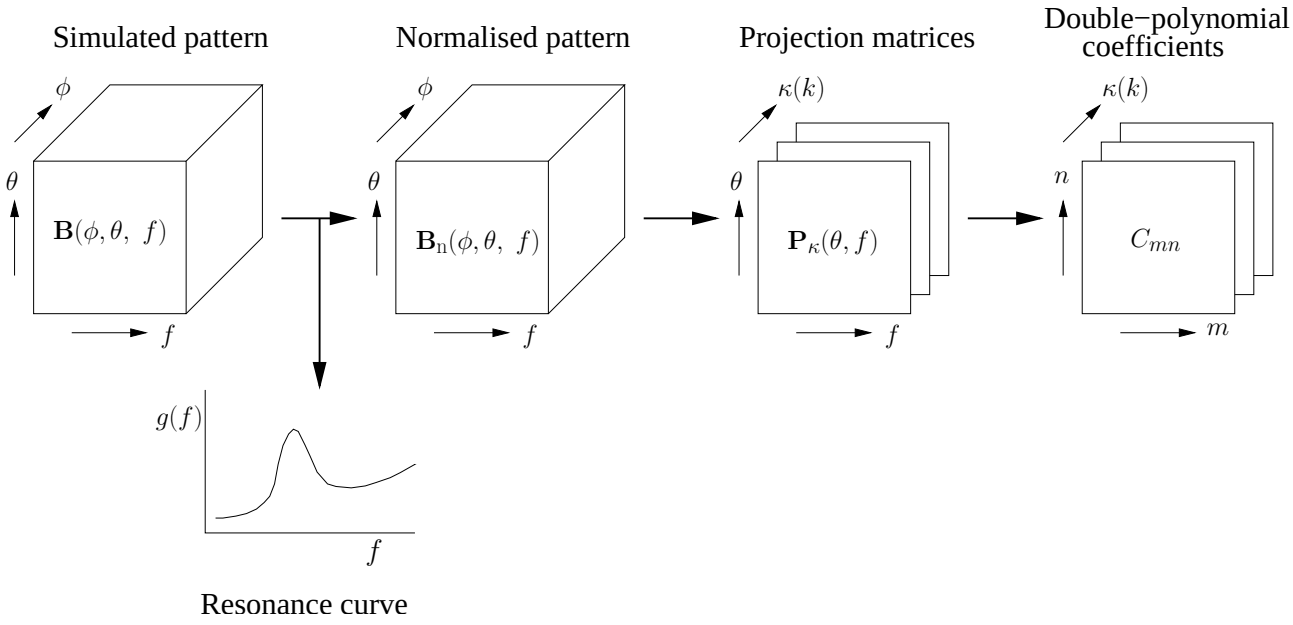

Figure 1: The analytic model: Components and fitting steps.

The basic components of the model and the fitting procedure are schematically shown in Fig. 1. The fit proceeds in three steps:

1. The overall dependence of gain on frequency is extracted by normalising the zenith values of the pattern $\mathbf{B}(\phi,\theta,\ f)$ to unity.

2. Amplitudes $\mathbf{P}(\theta, f)$ of azimuthal harmonics are fitted to the normalised pattern for all simulated values of θ and f.

3. The coefficients C_{mn} of a double polynomial in θ and f are fitted to the values $\mathbf{P}(\theta, f)$ of the harmonics amplitudes.

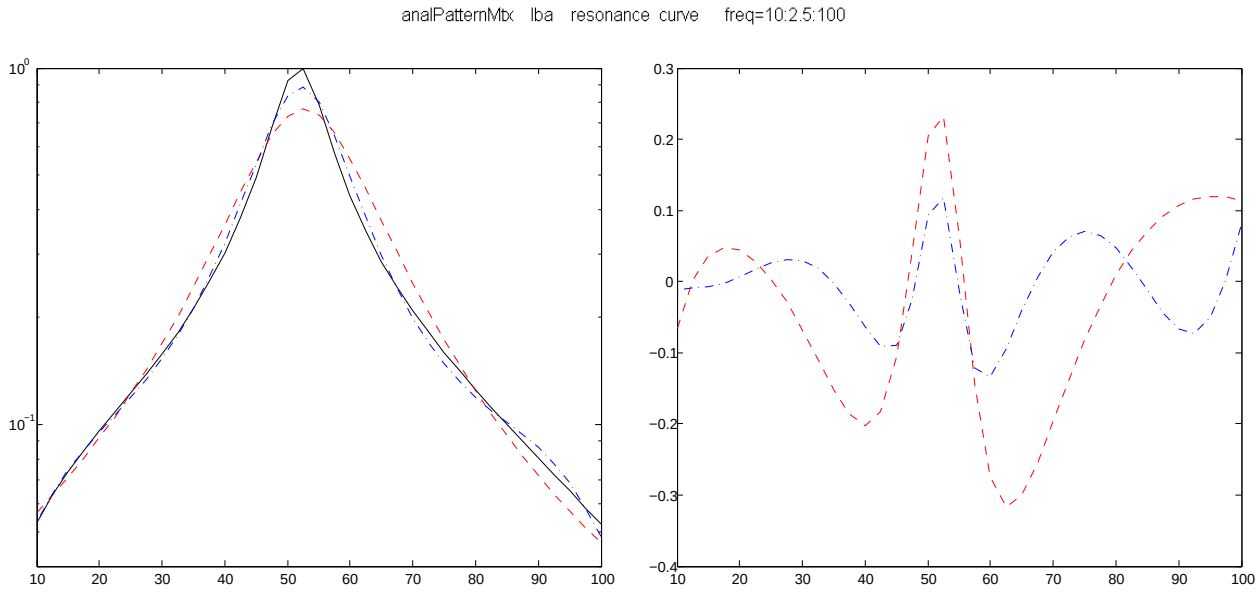

Figure 2: Fitting the resonance curve

The left panel shows, on a logarithmic scale, the reciprocal of the resonance curve and two weighted polynomial fits to it. Drawn black: $1/g_{\rm res} \approx 1 - (f - f_{\rm res})^2$*; dashed red: fitted parabola; dash-dotted blue: 4th-degree fit. The right panel shows the residuals for the resonance curve itself.*

5.1 Overall frequency dependence

In order to make the details of the antenna pattern accessible with simple functions, we begin with removing the overall frequency dependence which acounts for gain variations by an order of magnitude over the design band. An obvious way to try achieving this is by normalising the simulated antenna patterns per frequency point to unity at the zenith.

The gain curve thus obtained represents the guesstimated features remarkably well: Far from resonance, at the low and high ends of the band, the gains are closely proportional to f^2. Accomodating this dependence and the mid-band resonance:

$$\mathbf{G} \propto g_f \; g_{\rm res}; \qquad g_f \propto f^2; \quad g_{\rm res} \propto \frac{1}{x + (f - f_{\rm res})^2} \propto \frac{f^2}{a + bf + cf^2} \tag{1}$$

(Note that we are only interested in the frequency dependence, without attempting to represent constant scale factors.)

The fitting procedure is further discussed in App. B.2. Fig. 2 shows the result. The fit is seen not to be very accurate. It could be improved by raising the polynomial orders in the numerator and/or the denominator of Eq. (1). It may well be, though, that the present approximation is good enough in practice.

5.2 Dipole geometry

We now consider the beam for a single dipole normalised to unity gain at the zenith. Fig. 3 shows the three coordinate systems that we use:

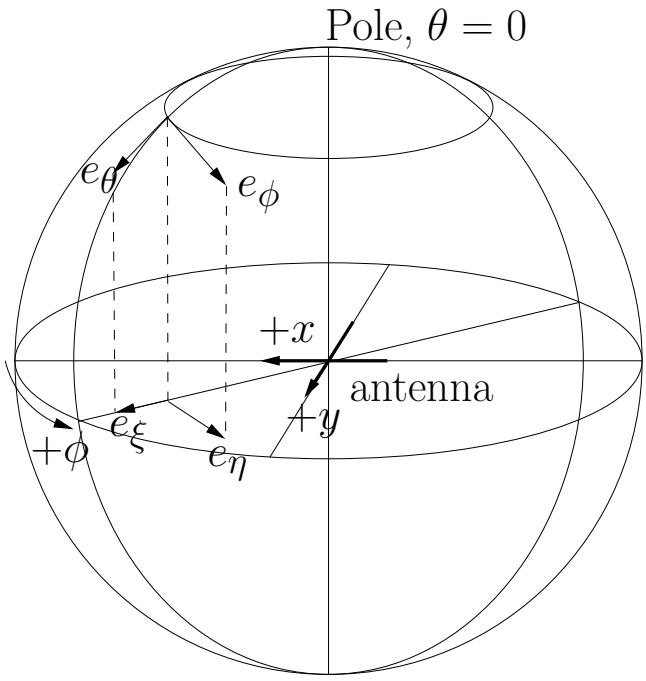

Figure 3: Observing geometry for one dipole.

See text.

- Sky directions are defined in a topocentric spherical system whose coordinates are *zenith angle* θ and *azimuth* ϕ. (We follow the antenna group in using zenith angle rather than elevation.) For any direction in the sky, the vector amplitude of the incident transversal radiation is $\mathbf{e}_{\theta\phi} = \begin{pmatrix} e_\theta \\ e_\phi \end{pmatrix}$.
- The horizontal xy frame defined by the antenna. We represent each dipole by a horizontal vector whose direction is that of the parallel horizontal electric field that produces a *positive* output amplitude. Azimuth is defined relative to the direction of the x dipole vector; the y dipole is in azimuth $\pi/2$.
- These two systems are connected by a horizontal $\xi\eta$ frame the axes of which are defined by the projections of e_θ and e_ϕ. It is a cartesian frame that is rotated relative to the xy frame over the azimuth ϕ. The projected field components are e_ξ and e_η.

A peculiarity of a spherical coordinate system is that it has a singularity at its Poles: In these directions the longitudinal coordinate and hence any function of it are multi-valued. The only generally safe way to avoid this problem in numerical calculations is to choose a coordinate raster that avoids the Poles; in our case, offset any raster that includes $\theta = 0$ by some negligibly small quantity.

5.3 Azimuth and dipole-vector definitions

As will be argued in Sec. 5.5 the formulae in this entire document are independent of the direction chosen for the azimuth. This document defines it as North over West, in order to define the XY coordinate system with the standard counter-clockwise position angle that also underlies the Stokes-parameter definitions.

Astronomers, however, define azimuth as North over East. The simplest way to reconcile the two definitions is to define the azimuth ϕ in this document as the opposite of the astrponmical azimuth.

One other item to be settled is the signs of the two dipole ouput voltages: If the X dipole is aligned North-East, then is the Y dipole aligned North-West or Souh-East? The asnwer affects the signs of Stokes U and V.

5.4 The short dipole and dipole pair

The basic concepts are best illustrated using the *short dipole* as a model. By *short* we mean that the dipole's length $l \ll \lambda$, so that propagation delays along this length are negligible. Under this condition, the dipole responds only to the field component that is parallel to it.

A *short antenna* is composed of two horizontal short dipoles, labeled x and y. For a free-floating dipole, the horizontal field $\mathbf{e}_{\xi\eta}$ is the geometric projection of the incident field onto the horizontal plane:

$$\mathbf{e}_{\xi\eta} = \begin{pmatrix} e_\xi \\ e_\eta \end{pmatrix} = \mathbf{P}\,\mathbf{e}_{\theta\phi}; \tag{2}$$

$\mathbf{P}$ projects e_θ onto e_ξ and e_ϕ onto e_η, so $\mathbf{P}$ is an elevation-dependent diagonal matrix:

$$\mathbf{P}(\theta) = \begin{pmatrix} p_{\theta\xi}(\theta) & 0 \\ 0 & p_{\phi\eta}(\theta) \end{pmatrix}. \tag{3}$$

In the absence of any obstacles

$$p_{\theta\xi} = \cos\theta; \qquad p_{\phi\eta} = 1. \tag{4}$$

In the presence of a ground plane, Eq. (2) is still valid, but its elements depend on θ in a more complicated way depending on the details of the geometry.

The transformation from $\mathbf{e}_{\xi\eta}$ to $\mathbf{e}_{\mathrm{xy}}$ is a coordinate rotation:

$$\mathbf{e}_{\mathrm{xy}} = \mathbf{R}(\phi)\,\mathbf{e}_{\xi\eta}; \qquad \mathbf{R}(\alpha) = \begin{pmatrix} \cos\alpha & -\sin\alpha \\ \sin\alpha & \cos\alpha \end{pmatrix} \tag{5}$$

Combining the above expressions and representing the x, y output pair as a column vector $\mathbf{v}$, we get

$$\mathbf{v}(\theta,\phi) = \begin{pmatrix} v_x(\theta,\phi) \\ v_y(\theta,\phi) \end{pmatrix} = \mathbf{J}(\theta,\phi)\,\mathbf{e}_{\theta\phi}(\theta,\phi); \qquad \mathbf{J}(\theta,\phi) = \mathbf{R}(\phi)\,\mathbf{P}(\theta) \tag{6}$$

The *rotation matrix* $\mathbf{R}$ and *projection matrix* $\mathbf{P}$ that we have introduced here will play a prominent rôle in the following discussions.

We shall return to the dipole pair before long, but now first consider a single dipole on its own.

5.5 Dipole-pattern symmetries and series expansions

We consider the symmetries that must exist in the response of our antenna, whether it be composed of short or of real-life dipoles. We assume that mechanically each dipole is symmetric w.r.t. the vertical and that it is essentially confined to a vertical plane (i.e. it is *thin* in the same sense that the term *short* was used earlier). The ground reflector is assumed to have the same symmetry.

We define a column vector[1] $\mathbf{p}_{\mathrm{x}}$ that describes the x dipole's response, v_{x}, to $\mathbf{e}_{\theta\phi}$:

$$\mathbf{p}_{\mathrm{x}}(\theta,\phi) = \begin{pmatrix} p_\theta(\theta,\phi) \\ p_\phi(\theta,\phi) \end{pmatrix}; \qquad v_{\mathrm{x}}(\theta,\phi) = \mathbf{p}_{\mathrm{x}}^\dagger(\theta,\phi)\;\mathbf{e}_{\theta\phi}(\theta,\phi). \tag{7}$$

The dipole will not respond to a field perpendicular to its vertical plane $\phi = 0$. Furthermore, it cannot distinquish directions that are mirror-image pairs w.r.t. this plane, so the sensitivities in such direction pairs are equal. For

[1] The symbol pair $\mathbf{P}$, $\mathbf{p}$ represented a projection earlier in this Note; the rationale for re-using them here will soon become clear. Note that $\mathbf{p}$ is not a geometrical vector in the proper mathematical sense. Given the response vector $\mathbf{p}_{\mathrm{x}}$ for the x dipole, $\mathbf{p}_{\mathrm{y}}$ does not follow from a $\pi/2$ geometrical rotation, but rather from a shift of its argument (cf. Sec. 6).

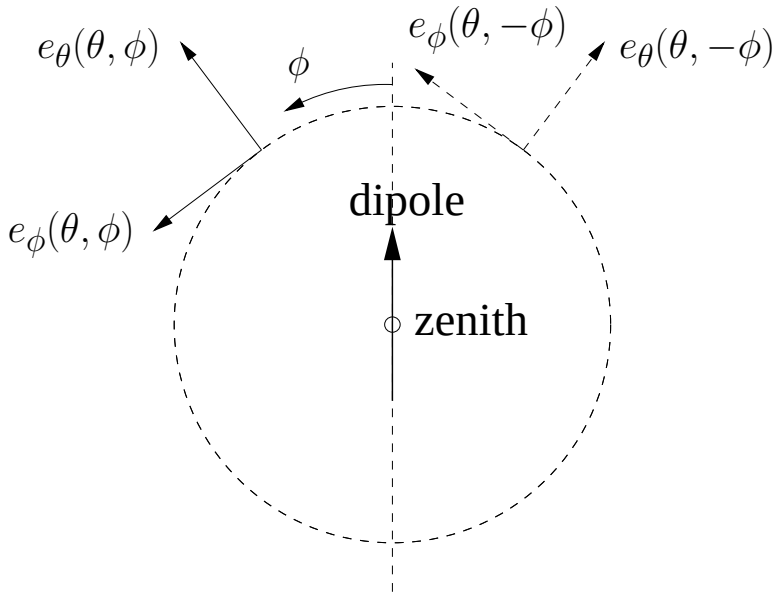

Figure 4: Symmetry properties of a symmetric dipole in a vertical plane.
/antennas/symmetries

The dipole is confined to the vertical x plane and symmetric w.r.t. the zenith direction.
Shown are the (projections of) the field components at positions (θ,ϕ) and $(\theta,-\phi)$. The dipole output voltage in response to these fields and the consequent symmetry properties of the response patterns are discussed in the text.

the fields shown in Fig. **??**, it follows that p_θ and p_ϕ are, respectively, even and odd in ϕ. Moreover, p_ϕ and p_θ change signs for an azimuth shift π. These properties dictate the series expansion

$$\begin{aligned} p_\theta(\theta,\phi) &= \sum_{k=0} p_{\theta,k}(\theta)\cos(2k+1)\phi \\ p_\phi(\theta,\phi) &= \sum_{k=0} p_{\phi,k}(\theta)\sin(2k+1)\phi \end{aligned} \tag{8}$$

Note that the p_0 coefficients have opposite signs, because, in the zenith

$$e_\phi(\theta,\phi) \equiv e_\theta(\theta,\phi+\pi/2), \tag{9}$$

An interesting consequence of the azimuthal symmetries is that the numerical values of the dipole pattern are independent of whether ϕ is defined to run clockwids or anti-clockwise. Indeed, flipping the direction does not affect p_θ and it reverses the signs of both ϕ (and hence of p_ϕ) and e_ϕ: We can use simulated data without having to know which way ϕ was defined for them.

6 The dual-dipole antenna

The antenna consists of two mutually perpendicular identical dipoles labeled x and y. The x dipole is situated in a symmetry plane of the y dipole; any radiation the former emits symmetrically impinges on the latterr and therefore cannot induce any currents in it. Thus the two dipoles (when properly aligned) operate in mutual independence.

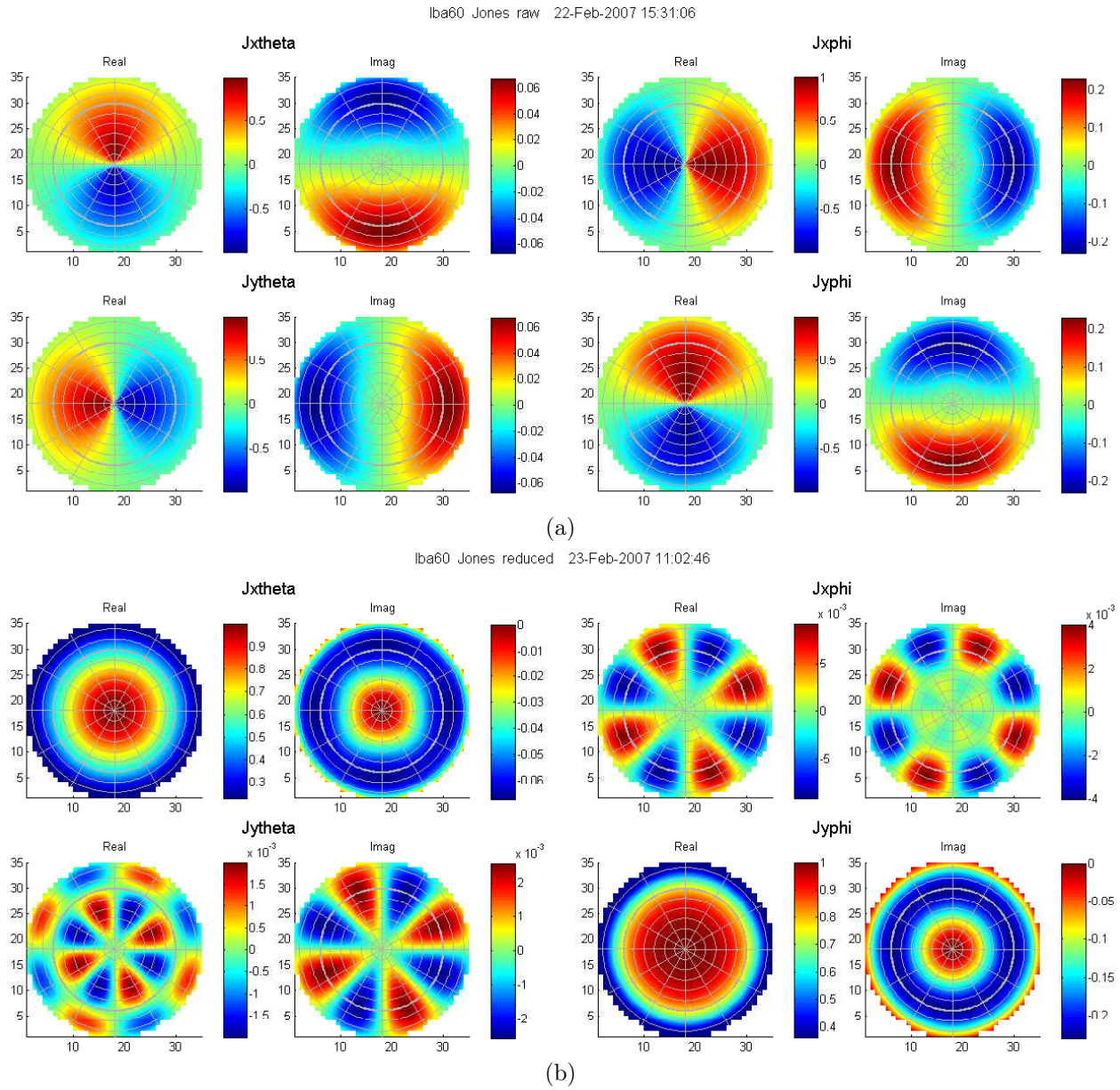

Figure 5: The raw and reduced Jones matrices as functions of direction for a simulated LBA antenna at 60 MHz.

The diagram is composed of two panels, labeled (a) for the raw and (b) for the reduced Jones matrix. Each shows the pair of real and imaginary parts for each of the four Jones-matrix elements as functions of topocentric coordinates. The scale is normalised to the zenith response, $J_{x\theta}(0,0) = 1$. The polar grid has an increment of 30 deg for azimuth ϕ, 10 deg for zenith angle θ. The $+x$ axis, $\phi = 0$, is toward the top.

In the raw matrix, the corresponding elements in the first and second rows are identical except for a $\pi/2$ rotation in azimuth. The sine and cosine symmetries of the fundamental ϕ harmonic are clearly visible in all four elements of $\mathbf{J}$.

In the reduced matrix, the diagonal elements are dominant. The 4-fold symmetry of the higher harmonics is visible in a slight non-circularity of the central pattern area. The off-diagonal elements are at a level of a few 10^{-3}, with a dominant $\sin 4\phi$ pattern.

6.1 Series expansion in azimuth for the Jones-matrix beam

The y dipole in position $+\pi/2$ has the same response in its own coordinate frame; in that frame, the azimuth is rotated over $-\pi/2$. Hence, from Eq. (8) the Jones matrix for the pair is

$$\mathbf{J}(\theta,\phi) \quad = \quad \begin{pmatrix} \mathbf{p}_x^\dagger \\ \mathbf{p}_y^\dagger \end{pmatrix} = \begin{pmatrix} p_\theta(\phi) & p_\phi(\phi) \\ p_\theta(\phi - \pi/2) & p_\phi(\phi - \pi/2) \end{pmatrix} =$$

$$
\begin{aligned}
&= \sum_{k=0} \begin{pmatrix} p_{\theta,k}\cos(2k+1)\phi & p_{\phi,k}\sin(2k+1)\phi \\ p_{\theta,k}\cos(2k+1)(\phi-\pi/2) & p_{\phi,k}\sin(2k+1)(\phi-\pi/2) \end{pmatrix} = \\
&= \sum_{k=0} \begin{pmatrix} p_{\theta,k}(\theta)\ \cos(-)^{k+1}(2k+1)\phi & (-)^{k+1}p_{\phi,k}(\theta)\ \sin(-)^{k+1}(2k+1)\phi \\ p_{\theta,k}(\theta)\ \sin(-)^{k+1}(2k+1)\phi & (-)^{k+1}p_{\phi,k}(\theta)\ \cos(-)^{k+1}(2k+1)\phi \end{pmatrix} \\
&= \sum_{k=0} \mathbf{R}\big(\,\kappa(k)\,\phi\,\big)\ \mathbf{P}_k(\theta), \qquad (10)
\end{aligned}
$$

where

$$
\begin{aligned}
\kappa(k) &= (-)^{k+1}\,(2k+1) \\
\mathbf{P}_k(\theta) &= \begin{pmatrix} p_{\theta,k}(\theta) & 0 \\ 0 & (-)^k\,p_{\phi,k}(\theta) \end{pmatrix}. \qquad (11)
\end{aligned}
$$

Whereas the above treatment yields a precise form for the azimuth dependence, the form of the projection matrices $\mathbf{P}_k$ remains unspecified. As in the case of the short dipole, it depends on the details of the antenna geometry: shape of the dipole, height above the ground reflector and shape of that reflector. For the LOFAR antennas, we must derive it from electromagnetic beam simulations; this will be discussed in Sec. 7.

For the sequel it is convenient to represent the set $\{\kappa\}$ by an arithmetic sequence with increment 4:

$$\{\kappa\} \equiv \{\ldots, -7, -3, +1, +5, \ldots\} \qquad (12)$$

Recall that the only assumptions made concern the symmetries in the antenna configuration, so the above derivation is quite general. The detailed geometry of the individual dipoles and the ground plane that together make up the antenna is contained in the functions $p_{\theta,k}(\theta)$ and $p_{\phi,k}(\theta)$. Since they depend on k and we do not know their forms, a separation of the variables θ and ϕ in the sum $\mathbf{J}$, as in Sec. 5.2, is no longer possible. Yet the individual terms in the series have the form of Eq. (6). The 0-order terms represents an 'ideal' antenna composed of short dipoles. The higher-order terms embody the way the actual antenna differs from this ideal; they must vanish in the short-dipole limit, i.e. at the lowest frequencies.

The diagrams in this document have all been produced through evaluation of Eq. (10) and the representation of the $\mathbf{P}_k$ to be discussed in Sec. 7. Fig. 5 shows a complex beam on a Cartesian grid. Fig. 6 is a plot of the higher-order k terms only, representing the deviations of the true antenna from the short-antenna ideal

The top part of Fig. 5 shows the responses of a typical antenna as a function of azimuth and elevation. Some version of a simulated LBA antenna is used as an example; the other antenna types developed for LOFAR follow the same basic pattern (a kinked dipole) and the example shown is quite representative. A general feature of these designs proves to be that their higher harmonics are weak — amplitudes well below 10% of the fundamental even at the top end of their frequency bands.

6.2 Azimuth-tracking of point sources

W.r.t. the sky field being observed, the xy coordinate system of Fig. 3 is entirely arbitrary. A logical first step in the processing of data is to rotate the data back to the $\xi\eta$ coordinate frame which tracks the field-centre azimuth ϕ_0. The required rotation $\mathbf{R}(-\phi_0)$ defines a virtual azimuth-tracking beam $\mathbf{J}'$:

$$\mathbf{J}'(\theta,\phi;\phi_0) = \mathbf{R}(-\phi_0)\ \mathbf{J}(\theta,\phi) = \sum_{k=0} \mathbf{R}\big(\,\kappa(k)\,\phi - \quad 1 \quad \phi_0\,\big)\ \mathbf{P}_k(\theta) \qquad (13)$$

Almost the same effect would be achieved by mechanically rotating the antenna to track ϕ_0:

$$\mathbf{J}''(\theta,\phi;\phi_0) = \quad \mathbf{J}'(\theta,\phi-\phi_0) \quad = \sum_{k=0} \mathbf{R}\big(\,\kappa(k)\,\phi - \kappa(k)\,\phi_0\,\big)\ \mathbf{P}_k(\theta) \qquad (14)$$

Since $\kappa(0) = 1$, the difference is only in the higher harmonics.

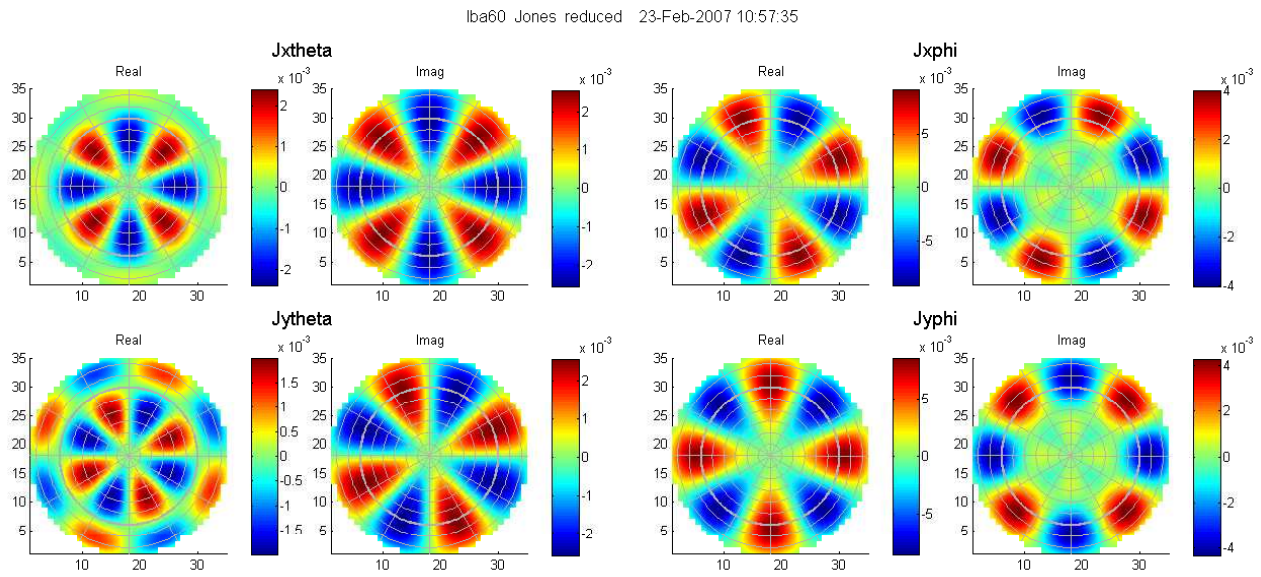

Figure 6: The higher-order terms in the pattern of the reduced beam of Fig. 5(b).

These patterns show how the real antenna deviates from the corresponding ideal short antenna. The diagonal and off-diagonal elements show $\cos 4\phi$ *and* $\sin 4\phi$ *patterns, respectively. (The off-diagonal patterns are the same as those in Fig. 5.)*

6.3 The Reduced Beam

It is interesting to study the *reduced* beam defined as

$$\mathbf{J}_{\mathrm{red}}(\theta,\phi_0) = \mathbf{J}'(\theta,\phi_0;\phi_0) = \sum_{k=0} \mathbf{R}\big(\,(\kappa(k)-1)\,\phi_0\,\big)\;\mathbf{P}_k(\theta) \tag{15}$$

Rather than the odd harmonics of Eq. (12) the reduced beam contains only 4-fold harmonics, representing a fourfold symmetry in azimuth. Obviously, this reflects the antenna's basic geometry, in which the four dipole arms are entirely equivalent. The definition of $+x$ and $+y$ directions that are tied to the antenna's output connections breaks this symmetry, but beam reduction restores it by detaching the antenna from the xy coordinates. In the case of the short antenna, only the $k = 0$ harmonic remains, so even the orientation of the antenna evaporates. For the real antenna, it remains present in the orientation of the higher-order terms.

For the 0-order harmonic, $\mathbf{R}(0\phi)$ is an identity matrix; the corresponding term in Eq. (15) reduces to the diagonal matrix $\mathbf{P}_0(\theta)$. In the complete sum, the diagonal elements ($x\theta$ and $y\phi$) of $\mathbf{J}_{\mathrm{red}}$ are dominated by $\mathbf{P}_0$ which has the same value for all azimuths; the higher harmonics are recognisable as small deviations from circularity with 4-fold symmetry. In the off-diagonal elements, the 0-order contribution is absent; there is only the 4-fold pattern of higher harmonics — at their much lower level. The latter is also true for the diagonal elements if we suppress the fundamental term in Eq. (15).

All of these features are on display in Figs. 5 and 6.

7 Elevation and frequency dependencies and their analytic representation

The dependences of the beam on zenith angle are repesented by the projection matrices $\mathbf{P}_k(\theta)$ in Eqs. (10) and (11)). These are also functions of frequency f. Theory does not readily suggest a suitable set of basis functions; anyway, if such a set should exist, it would most probably entail complicated transcendental expressions whish are computationally expensive to apply.

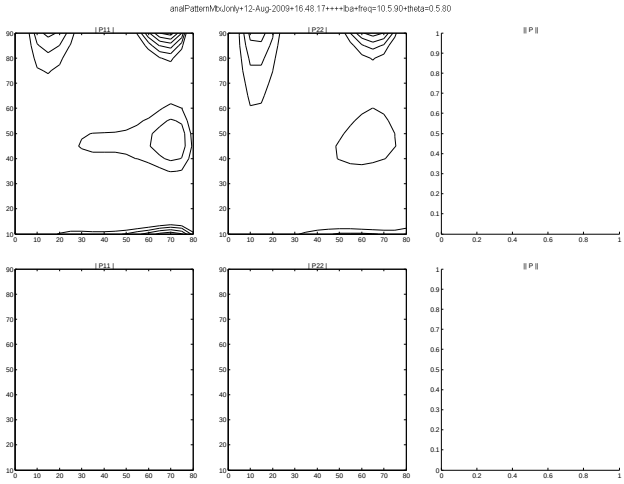

Figure 7: Residuals of the $(\theta,\ f)$ fit for the LBA antenna.

θ in degrees is on the horizontal axis, f in MHz on the vertical axis. Shown are the absolute values of the two nonzero elements and of the Frobenius norm $\sqrt{p_{11}^2 + p_{22}^2}$ of the matrix $\mathbf{P}$ for $\kappa = 1$.

The polynomial degrees used in Eq. (16) are $M = 4$ for θ and $N = 3$ for f. Contour level is .5% relative to the normalised beam peak value of unity.

We therefore opt for a simple double-polynomial expansion[2]:

$$\mathbf{P}_k(\theta; f) = \sum_{m,n} p_{kmn}\, \mathbf{T}_{km}(\theta)\, F_{kn}(f) \tag{16}$$

Each of the elements of each $\mathbf{P}_k$ is a function of the form Eq. (16) that is independent of the others. The $\mathbf{P}_k$ being diagonal matrices, we have to apply two independent fits per k harmonic.

8 Observing point sources

8.1 Measurement Equation

So far we have considered a single antenna. When two antennas kabeled j and k are combined in an interferometer to measure a component $\mathbf{C}_{jk}$ of the coherency, the *Measurement Equation* applies:

$$\mathbf{C}'_{jk} = \mathbf{J}_j\, \mathbf{C}_{jk}\, \mathbf{J}_k^\dagger \tag{17}$$

.

8.2 Stokes vector and Mueller-matrix beam

The Stokes vector on the sky consists of 4 elements, each of which represents a brightness:

$$\mathbf{s} = \begin{pmatrix} I & Q & U & V \end{pmatrix}^{\mathrm{T}}. \tag{18}$$

It is a one-to-one alias of the coherency matrix, defined by the identity

$$\mathbf{C} \equiv \begin{pmatrix} I+Q & U+iV \\ U-iV & I-Q \end{pmatrix}. \tag{19}$$

[2]A product of two polynomials, one in θ and one in f, would provide an even simpler representation. It was found in practice to be too inflexible to yield a good fit.

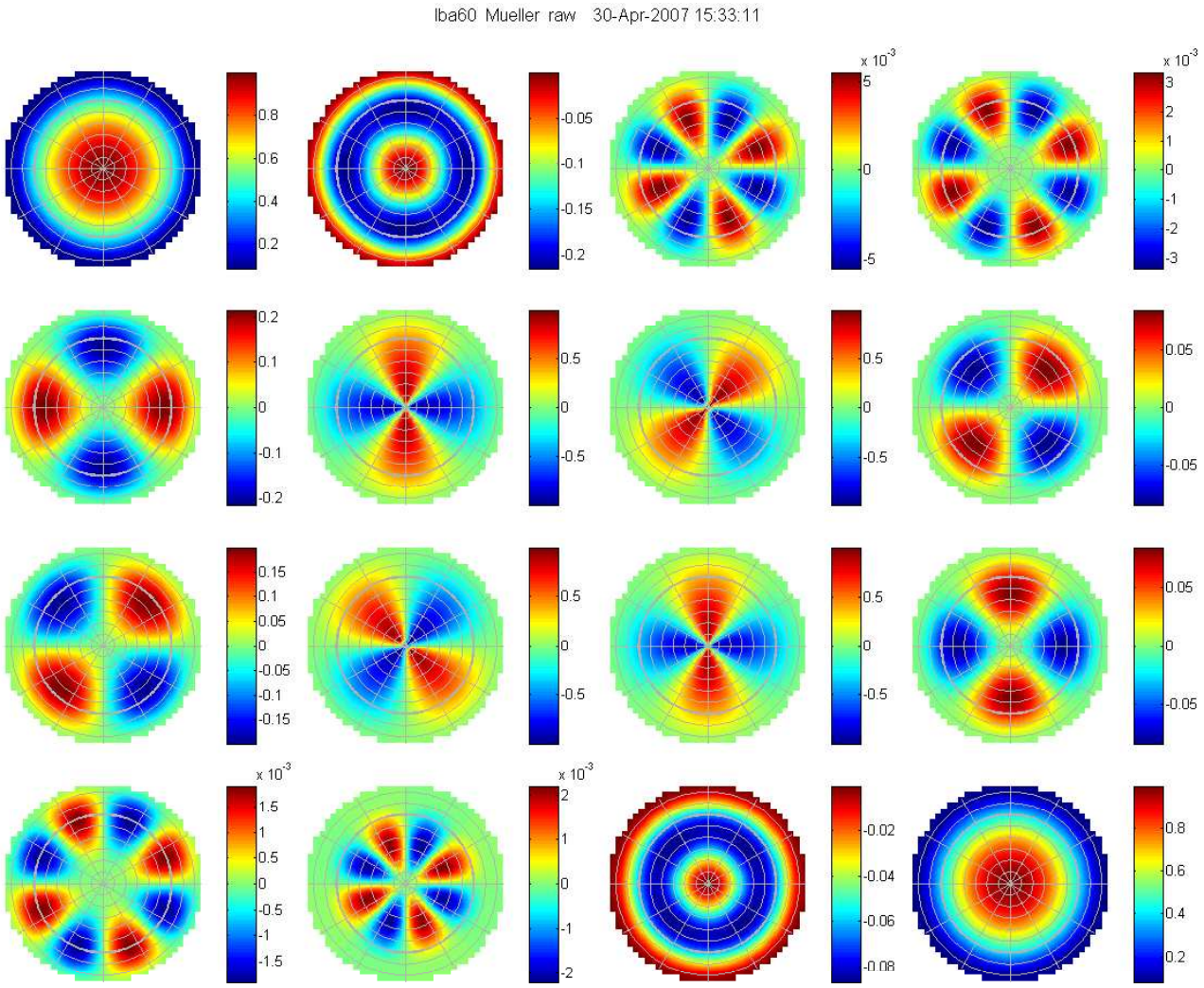

Figure 8: The Mueller-matrix corresponding to the raw Jones-matrix beam of Fig. 5

The 16 beams are arranged like the elements of the matrix $\mathbf{M}$ *in Eq. (20).*

In terms of the Stokes vector, the Measurement Equation Eq. (17) becomes

$$\mathbf{s}'_{jk} = \mathbf{M}(\mathbf{J}_j, \mathbf{J}_k)\ \mathbf{s}_{jk}, \tag{20}$$

where $\mathbf{M}$ is the 4×4 *Mueller matrix*. For a *homogeneous interferometer*, i.e. $\mathbf{J}_j \equiv \mathbf{J}_k$, $\mathbf{M}_{jk}$ is real. In this case the 16 elements of M are interdependent: Only 7 real parameters are required to define the matrix, and $\mathbf{M}_{jk}$ is the polarimetric equivalent of the power beam for a scalar interferometer.

There are several ways of calculating $\mathbf{M}$ form its arguments $\mathbf{J}_j,\ \mathbf{J}_k$. Fig. 8 shows the Mueller-matrix beam corresponding to Fig. 5(a);

8.3 The rotating sky and parallactic rotation

So far we have considered the source in topocentric zenith-angle/azimuth coordinates. The sources that we actually observe are carried around through the antenna beam by the Sky's (apparent) rotation. Consequently, we must consider the transformation from Equatorial celestial coordinates to our topocentric system.

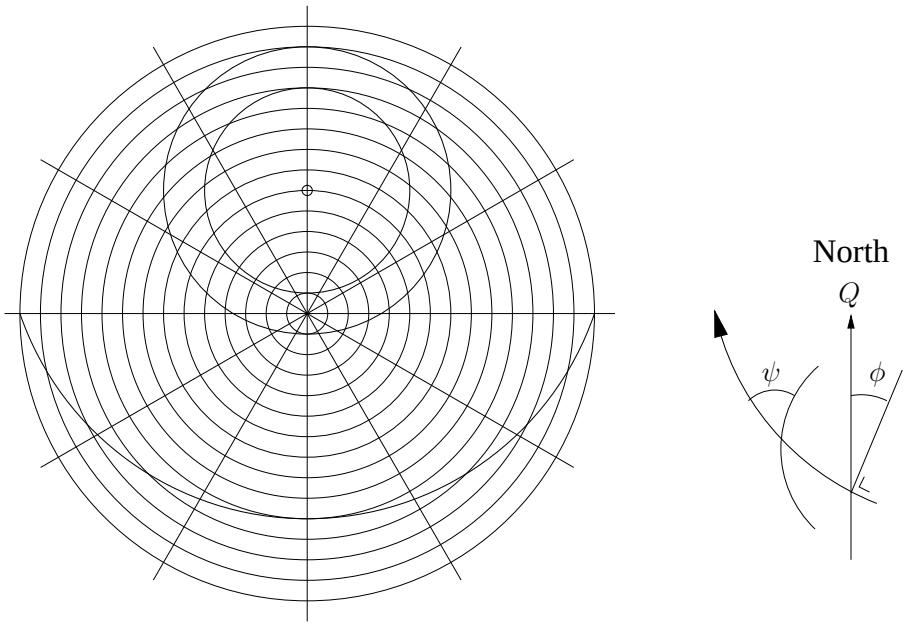

Figure 9: Schematic of the Sky with representative source tracks.

The Sky is shown projected onto the horizontal plane; the geometry shown is strongly distorted radially except near the zenith at the centre of the figure. The thin circles are topocentric latitude circles, θ =constant, the heavy circles are source tracks with δ =constant. In celestial coordinates, the direction of positive Stokes Q is defined to be toward the Pole. In xy antenna coordinates, it is in the $+x$ direction (with which the $+Q$ direction coincides by definition). ϕ is the azimuth and ψ the parallactic angle.

In a sidereal day, the θ direction rotates uniformly to make a full turn; its projection, moving non-uniformly, also makes a full turn. The true three-dimensional geometry further complicates the matter, but the basic conclusion stands that the output xy vector must make a full turn. Apart from this, its amplitude decreases with hour angle away from culmination due to the decreasing antenna gain.

At culmination, the projection of the source's θ field component is aligned North-South. Stokes Q on the sky is aligned with θ, in the projection it is North-South; so we expect a pure positive Q output at upper culmination, $\phi = \pi$ — and hence also at lower culmination $\phi = 0$.

The celestial position of a source at any time is described by its hour angle H and declination δ. The transformation to (θ, ϕ), depending on geographic latitude λ, is given by well-known equations [3]:

$$\sin\theta\cos\phi = \cos\lambda\sin\delta + \sin\lambda\cos\delta\cos H \quad (21)$$

$$\sin\theta\sin\phi = \cos\delta\sin H \quad (22)$$

$$\cos\theta = \sin\lambda\sin\delta + \cos\lambda\cos\delta\cos H \quad (23)$$

For an unpolarized point source these are all we need.

For a linearly polarized source we must also consider the relative rotation between the Equatorial and topocentric grids at the source position. The angle of rotation ψ is known as the *parallactic rotation*; it is given by the formula

$$\tan\psi = \frac{\cos\lambda\sin H}{\sin\lambda\cos\delta - cos\lambda\sin\delta\cos H} \quad (24)$$

Both transformations are not only time-dependent; for an extended source they also vary with position in the source: They represent a time-dependent image-plane effect. Here, however, we confine ourselves to point sources.

[3] The formulae to be found in astronomical textbooks usually refer to the elevation or altitude a; by definition $\theta = \pi/2 - a$ and the l.h.ss. of our equations have been adapted accordingly.

The transformations Eqs. (23) and (24) operate in each direction on the Sky, but their effect is most dramatic near the zenith, as shown in Fig. 9. Both parallactic angle and azimuth vary rapidly as the source passes, and both affect the polarization direction measured at the antenna output. The crucial question is with which sign the effects combine.

To answer it, we consider the geometry as seen from the zenith and return to the concept (Sec. 5.4) of the antenna as a device projecting the sky field onto the horizontal plane. The caption of Fig. 9 discusses the effect of the projection.

For a purely Q-polarized source we qualitatively we expect the outputs

$$Q' \propto \cos 2\phi; \qquad U' \propto \sin 2\phi, \tag{25}$$

implying that near the zenith the wild effects of parallactic angle and azimuth variations cancel rather than reinforce each other. This suffices to determine the sign of the former effect.

Parallactic rotation is a gift of Nature that we cannot reject, like it or not. It is therefore proper to consider it as an inherent property of the antenna beam projected onto the Sky, which we do by including it as an extra factor in our beam model (with the appropriate definition for the sign of ψ):

$$\mathbf{J}_{\text{sky}} = \mathbf{J}_{\text{antenna}}\mathbf{R}(\psi) \tag{26}$$

Fig. 10(a) shows the resulting Mueller-matrix beam. From a comparison with Fig. 8 the imortance of parallactic rotation becomes quite clear.

8.4 Predicting Stokes outputs for a source track

For a source of given position ($H(t)$, δ) and Stokes vector, we can use our beam model to calculate the Stokes output as function of t. For demonstration purposes we may consider, e.g. the effect of Stokes Q alone, even though in reality it cannot exist without an $I > |Q|$.

This has been done, for a circumpolar source, to produce Fig. 10(b). The values in this quartet of graphs correspond to the values of the second (Q) column of $\mathbf{M}$ along the source track that is shown in predictStokes(a).

The Q and U outputs are in agreement with our predictions, Eq. (25); the I and V outputs represent some of the polarimetric errors of the antenna.

8.5 Antenna in arbitrary azimuth

In the preceding section the antenna was assumed to be with X aligned North-South. Actually, LOFAR antennas are positioned with X in the North-East and Y in the North-West direction. In terms of the coordinate definitions in Sec. 5.2 its azimuth is $\phi = -\pi/4$.

Since the output Stokes parameters are defined relative to the X direction, this rotation corresponds to a rotation over $-\pi/2$ of the Stokes QU polvector. In Fig. 10(a) this corresponds to a swap of the second and third collumns and a negation of one of them.

Appendix

A anecdotes

Examples of earlier results

B Numerical model fit to an antenna pattern

The residuals of the θ-Frequency fit.

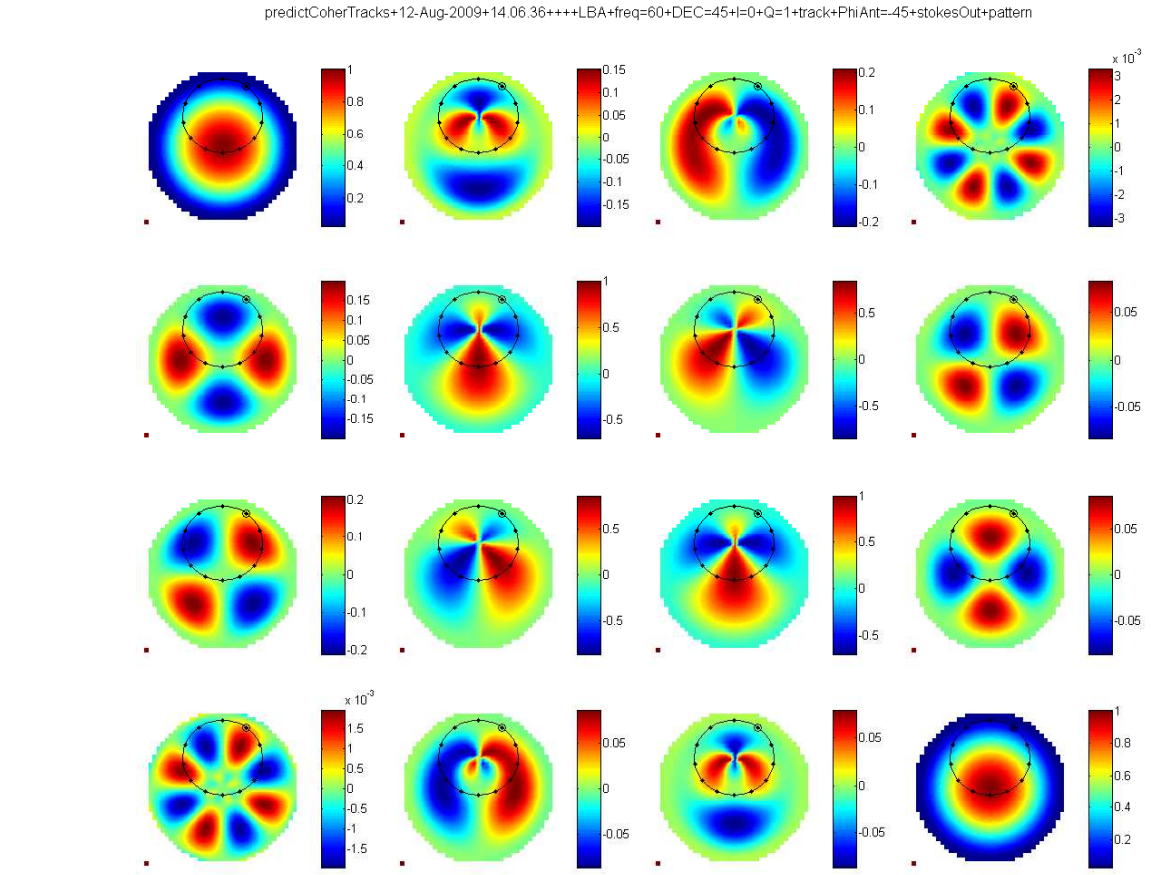

(a)

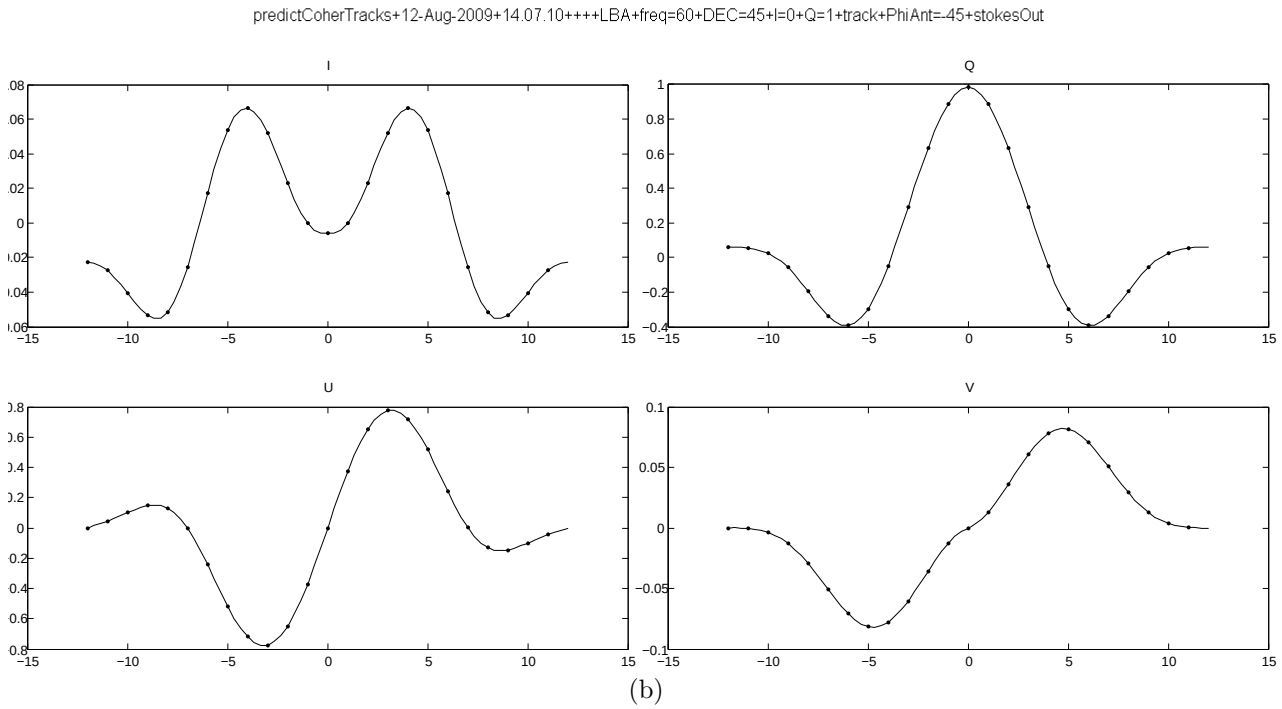

(b)

Figure 10: Simulated outputs of a LOFAR antenna for a fictitiously polarized point source.

The LBA antenna is positioned in azimuth 0. *To bring out the response to linear polarization, a non-physical intensity* $I = 0$ *is assumed. The frequency is 60 MHz.*

(a): The Mueller matrix as a function of (θ, ϕ). *The track of a source at* $\delta = 45^\circ$ *is superimposed, with markers at 1-hour intervals.*

(b): The Stokes-parameter outputs versus hour angle, demonstrating the behaviour predicted in Eq. (25). Towards larger hour angle (i.e.lower elevation) the responses are attentuated by the general attenuation of the antenna beam. The much weaker I *and* V *outputs are produced by poldistortion.*

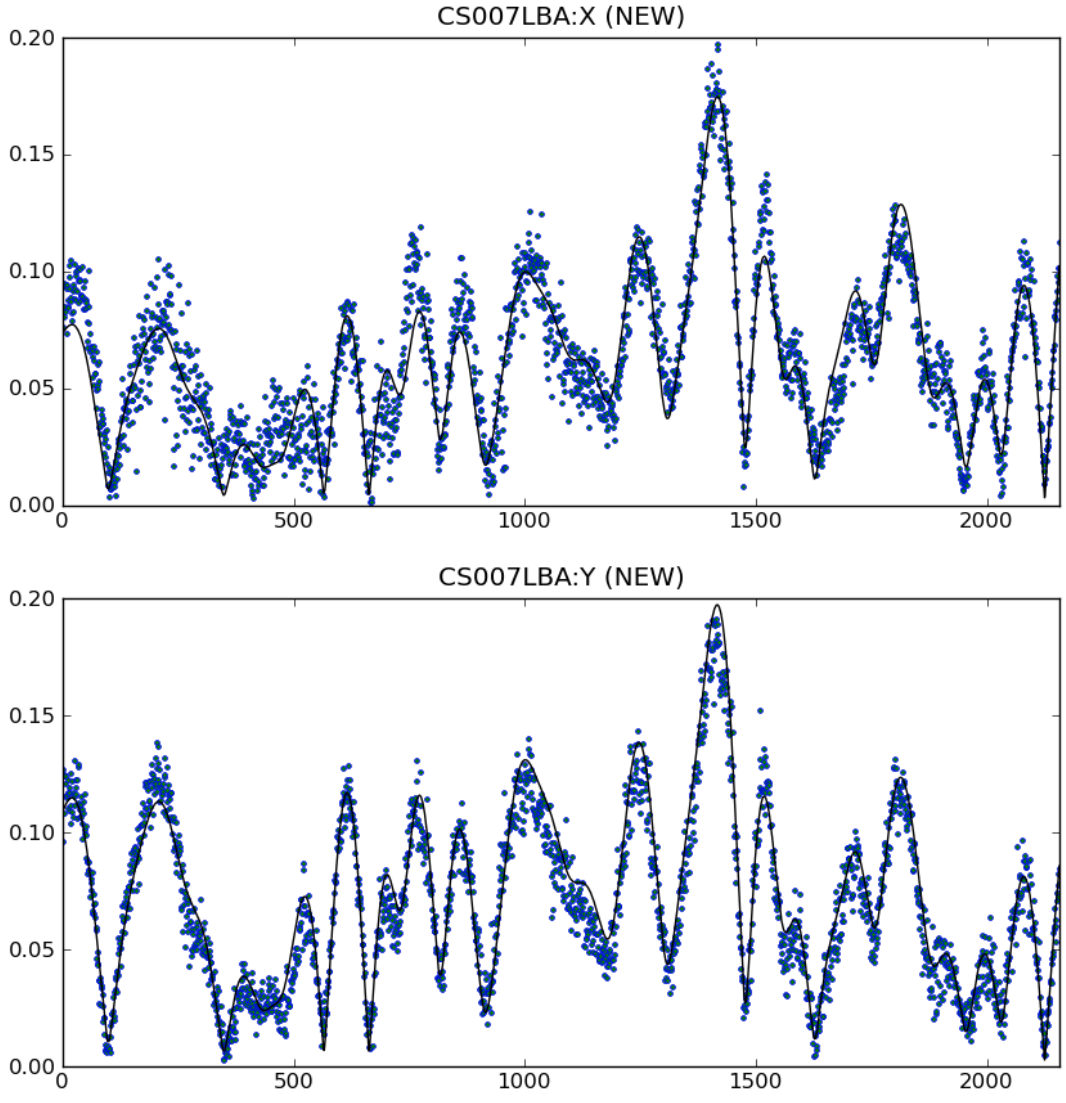
CS007LBA:X (NEW)
0.20
0.15
0.10
0.05
0.00
0
500
1000
1500
2000
CS007LBA:Y (NEW)
0.20
0.15
0.10
0.05
0.00
0
500
1000
1500
2000

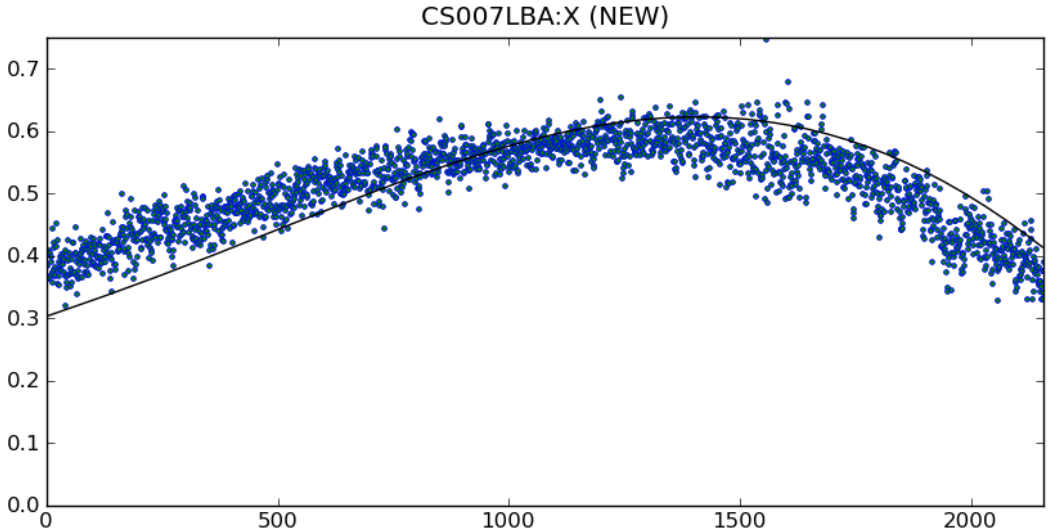
CS007LBA:X (NEW)
0.7
0.6
0.5
0.4
0.3
0.2
0.1
0.0
0
500
1000
1500
2000

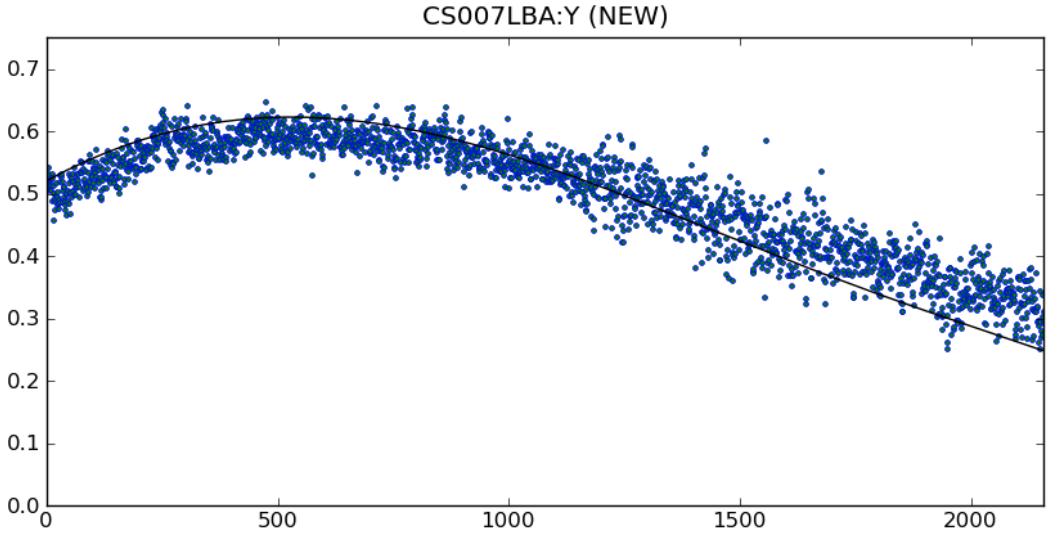
CS007LBA:Y (NEW)
0.7
0.6
0.5
0.4
0.3
0.2
0.1
0.0
0
500
1000
1500
2000

B.1 Minimising absolute residuals

This appendix outlines the algorithms for fitting the model of Secs. 6.1 and 7 and for calculating the model's value for arbitrary parameters θ, ϕ and f.

Given an array of $\mathbf{J}$ values calculated through e.m. simulation on a regular grid (θ, ϕ, f) the coefficients $\mathbf{P}_k(\theta, f)$ are calculated from Eq. (30) by an LSQ fit. Since the rotation matrices $\mathbf{R}_k(\phi)$ form an orthogonal basis in ϕ the calculation simplifies to

$$\mathbf{P}_k(\theta, f) = \sum_{\phi} \mathbf{J}(\theta, \phi, f)\ \mathbf{R}(-\kappa(k)\,\phi)\ /N_\phi \tag{27}$$

where N_ϕ is the number of ϕ values in the grid. From Sec. 6.1 we know that the $\mathbf{P}_k$ must come out diagonal. (Their failure to do so would indicate an error either in the simulated data or in the fitting algorithm.)

$\mathbf{C}^{\odot}_{k;\,m,n}$ is calculated through an LSQ fit for each diagonal element; the two fits are independent because all matrices involved are diagonal. Since off-the-shelf fit routines operate on scalars rather than 2×2 matrices, scalar fits must be performed for each k and either of the two diagonal elements of $\mathbf{P}_k$.

B.2 Minimising relative residuals

The minimising of the rms residuals distributes the errors indiscriminately over the entire beam; consequently the *relative* errors are inversely proportional to the beam and increase with zenith angle. Let us call the observation $O(\theta, \phi)$ and the fitted approximation $A(\theta, \phi)$, then the residuals that we really want to minimise are

$$r_{\text{relative}} = \frac{A(\theta, \phi) - O(\theta, \phi)}{O(\theta, \phi}. \tag{28}$$

This is easily realised my dividing both the observations and the basis functions by $O(\theta, \phi)$, which is equivalent to applying O as a weighting function[4].This weighting reduces the r.h.s. of the condition equations to all 1s and inflates the basis functions at higher θ. This works fine as long as O contains no values close to 0.

In our application suitable weights are the inverses of P for $k = 0$ because this term strongly dominates in Eq. (30) and the relative errors in the much smaller $k > 0$ terms are unimportant.

C Calculating Jones matrix values

The matrices $\mathbf{P}_k(\theta, f)$ are diagonal. Each element $p_{jj,k}$ is calculated with the corresponding coefficient matrix $[\mathbf{C}]_{jk}$:

$$p_{jj,k} = \bar{\theta}\ [\mathbf{C}]_{jk}\ \bar{f}. \tag{29}$$

where

- $\bar{\theta}$ is a row vector $\begin{pmatrix} \theta^0 & \theta^1 & \dots & \theta^{N_\theta} \end{pmatrix}$;
- $[\mathbf{C}]$ is a twodimensional array of $(N_\theta + 1) \times (N_f + 1)$ (columns $\times$ rows) matrices. The indices of the array are the j and k in Eq. (29); in computing code $[\mathbf{C}]$ is conveniently represented as a 4-D array.
- $\bar{f}$ is a column vector $\begin{pmatrix} f^0 & f^1 & \dots & f^{N_f} \end{pmatrix}^{\mathrm{T}}$;

Multiple values of θ and f can be processed in a single operation by stacking the corresponding vectors θ and $\mathbf{f}$ to form matrices.

The Jones matrices are evaluated from the equation

$$\mathbf{J}(\theta, \phi, f) \quad = \quad \sum_{k} \mathbf{R}(\kappa(k)\,\phi)\ \mathbf{P}_k(\theta, f) \tag{30}$$

[4]Instead of O, A could serve as numerator in Eq. (28), but we do not know it a priori. In most practical cases (anyway those we are interested in) the differences between the two functions (which are the residuals), will be small.

D Calculating Mueller matrices

Paper I shows that the Mueller matrix for an interferometer with arbitrary elements is derived from its Jones matrices by

$$\mathbf{M}_{jk} = \tfrac{1}{2}\ \mathbf{S}^{\dagger}\ \mathbf{J}_{j} \otimes \mathbf{J}_{k}^{*}\ \mathbf{S} \tag{31}$$

where $\mathbf{S}$ is a 4×4 unitary matrix constant.

An alternative formulation follows from Paper IV: Let the elements of the Stokes vector $\mathbf{s}$ be labeled 0 through 3 and be represented by their corresponding 2×2 Pauli matrices:

$$\mathbf{s} = \left(\begin{array}{cccc} \mathbf{s}_0 & \mathbf{s}_1 & \mathbf{s}_2 & \mathbf{s}_3 \end{array} \right) \tag{32}$$

with $\mathbf{s}_0 = \mathbf{I};\ \mathbf{s}_1 = \mathbf{Q}$; etc. Then the element pq of $\mathbf{M}_{jk}$ is given by

$$\mathbf{M}_{jk,pq} = \tfrac{1}{2}\mathrm{Tr}\ \ \mathbf{s}_{\mathrm{p}}\ \mathbf{J}_{j}\mathbf{s}_{\mathrm{q}}\ \mathbf{J}_{k}^{\dagger} \tag{33}$$

Either form may be written out in terms of the elements of the $\mathbf{J}$. Let

$$\mathbf{J}_{j} = \left(\begin{array}{cc} a & b \\ c & d \end{array} \right); \qquad \mathbf{J}_{k} = \left(\begin{array}{cc} p & q \\ r & s \end{array} \right), \tag{34}$$

then

$$2\mathbf{M} = \tag{35}$$
$$\left(\begin{array}{cccc} ap^* + bq^* + cr^* + ds^* & ap^* - bq^* + cr^* - ds^* & aq^* + bp^* + cs^* + dr^* & i(aq^* - bp^* + cs^* - dr^*) \\ ap^* + bq^* - cr^* - ds^* & ap^* - bq^* - cr^* + ds^* & aq^* + bp^* - cs^* - dr^* & i(aq^* - bp^* - cs^* + dr^*) \\ ar^* + bs^* + cp^* + dq^* & ar^* - bs^* + cp^* - dq^* & as^* + br^* + cq^* + dp^* & i(as^* - br^* + cq^* - dp^*) \\ -i(ar^* + bs^* - cp^* - dq^*) & -i(ar^* - bs^* - cp^* + dq^*) & -i(as^* + br^* - cq^* - dp^*) & as^* - br^* - cq^* + dp^* \end{array} \right)$$